

Manufacturing Letters

Manufacturing Letters 33 (2022) 744-751



50th SME North American Manufacturing Research Conference (NAMRC 50, 2022)

3D Printing of Largescale Functional Nanofilm using Electrically assisted Direct Ink Deposition

Yizhen Zhu^a, Banashree Gogoi^b, Pranith Alluri^a, Mitesh Suhas Despande^a, John Hutchins^a, Edem Tagbor^c, Terry L. Alford^d, Xiangjia Li^a*

^a Mechanical Engineering Graduate Program, School for Engineering of Matter, Transport and Energy, Arizona State University, Tempe, AZ, 85286, USA
^bSchool for Molecular Science, Arizona State University, Tempe, AZ, 85286, USA
^cMatterials Science and Engineering Graduate Program, School for Engineering of Matter, Transport and Energy, Arizona State University, Tempe, 47, 8528

Abstract

Functional nanofilms show significant importance for various applications in different fields, such as sustainable energy, biomedicine, electronics, and optics. However, there are still many challenges in the fabrication of nanostructured films with tailored properties using traditional manufacturing technologies. A novel 3D printing approach called electrical field-assisted direct ink deposition (EF-DID) was developed to produce large-scale nanofilms with controllable nanostructures and patternable features. In the proposed method, the formation of nanodroplets in the direct ink deposition was investigated under an electrostatic field with high voltage. Critical printing parameters, including solution concentration, deposition height, applied voltage, and ink flow rate, were studied systematically to understand fundamental mechanisms of the nanostructures generation during the printing. In addition, the scientific relationship between deposition parameters and nanofilm properties, including film thickness, electrical conductivity, and contact angle, were explored. Finally, patterned nanofilms with well-organized nanostructures were fabricated to demonstrate potential application prospects in the field of nanotechnology.

© 2022 Society of Manufacturing Engineers (SME). Published by Elsevier Ltd. All rights reserved. This is an open-access article under the CC BY-NC-ND license (http://creativecommons.org/licenses/by-nc-nd/4.0/) Peer-review under responsibility of the Scientific Committee of the NAMRI/SME. *Keywords:* 3D Printing; Nanofilm; Direct ink deposition; Largescale manufacturing; Conductive polymer

1. Introduction

Functional nanofilm has been widely used in various fields such as new energy, healthcare, robots, quantum science, and environmental engineering [1]. Many manufacturing technologies, including chemical/physical vapor deposition, conversion coating, plating, spraying, spin/dip coating, and roll to roll coating, have been developed to fabricate nanofilms using different types of materials [2]. Poly(3,4-ethylene dioxythiophene)-poly(styrene sulfonate) (PEDOT:PSS) is a conductive polymer that has been widely used for both commercial applications and fundamental research [3-4]. For

example, PEDOT:PSS has become one of the most popular polymers used as a transparent hole transport layer (HTL) in hybrid organic-inorganic solar cells [5]. High transparency in the visible range, excellent thermal stability, and tunable conductivity are some of the main advantages of PEDOT:PSS over other HTL materials [6-7]. Traditionally, the PEDOT:PSS nanofilm is fabricated using the spin coating technique [8-9]. Centrifugal force drives liquid material radially outward during the coating, and a thin residual film is retained on the flat substrate because of viscous force and surface tension. After that, the solvent is evaporated to form a nanofilm [8-9]. However, it is not easy to use the spin coating method to

^cMaterials Science and Engineering Graduate Program, School for Engineering of Matter, Transport and Energy, Arizona State University, Tempe, AZ, 85286, USA

^{*} Corresponding author. Tel.: +1 480 727 8612. E-mail address: xiangjia.li@asu.edu

fabricate nanofilms with large areas and patternable features due to the limitation of coating capability. The substrate dimensions that can be coated are typically around 10 mm² [8]. The roll-to-roll coating is an alternative nanofilm fabrication technology in solar cell manufacturing [10-11]. In the roll-to-roll coating, the coating material is first applied by one or more auxiliary rolls onto an application roll. The coating is wiped off the application roller by the substrate as it passes around the support roller at the bottom [12-13]. Large-area electronic devices can be fabricated using this approach [10-11]. However, it is hard to achieve multi-material coating, and the coating speed is no faster than 3 mm/s [10]. Besides, the roll-to-roll coating machine is more expensive than other manufacturing technologies.

Currently, several different types of three-dimensional (3D) printing methods have been developed to fabricate parts with nanofeatures, such as two-photon polymerization (TPP), electrostatic jet printing, and inkjet printing [14-15]. In the TPP process, a femtosecond laser beam is utilized to initiate the polymerization caused by the absorption of multiple photons [16]. However, the TPP process is time-consuming to fabricate nanoscale features in a large area since the laser beam has to scan the entire volume [16]. In addition, the material that can be printed using the TPP process limits its application in solar cell manufacturing [16]. Nozzle-based printing methods are also developed to accomplish the fabrication of nanofeatures. For example, inkjet printing is widely used to fabric nanofilms for flexible electronics [17]. Electrohydrodynamic jetting (EHD-jetting) utilizes the electric field to form droplets or fluid flows for delivering inks to a substrate [18]. However, nanofilms are built dot by dot or line by line by using nozzlebased printing processes so it is not time efficient to fabricate the large-scale product. An optimized EHD jetting process was developed by integrating an extra electrical field [19]. An additional electrical field was used to deflect the jet trajectory to control the location of the continuously jetted materials. The printing speed is improved dramatically compared with the traditional EHD jetting in which mechanical stages are used to achieve the motion [19]. However, even though the fabrication speed is critically increased, the printing area is restricted to a small area because of the limitation of deflection angle. The largest lateral size of an object that can be printed by jet deflection was around 2 mm without mechanical movement [19]. Besides, EHD is not ideal for nanofilm fabrication due to limited fabrication resolution since nano features are formed by stacking nanoscale lines. As a result, there are stair-effects on the surface of the printed object, and the property of printed nanofilm is anisotropic.

Even though there are some limitations, 3D printing provides a promising tool to construct nanostructures with advanced material for various applications [20-24]. It is necessary to develop a 3D printing technology to fabricate large-scale nanofilms with enhanced properties using advanced materials, which remains a critical challenge for advanced manufacturing research [25-26]. To address such a critical challenge, we demonstrate a novel 3D printing approach, named electrical field-assisted direct ink deposition (EF-DID), to fabricate large-area nanofilms within minutes. The electrical field generation module was integrated with direct ink writing

in the EF-DID process, which incorporated X/Y/Z motions and material extrusion module to deposit patternable nanofilm on subtracts. The largest achievable lateral dimension without any mechanical movement assisting is around 30 mm, 15 times the largest lateral size accomplished in the optimized EHD jetting process [19]. Any film smaller than 30 mm can be printed within 30 seconds by our proposed EF-DID. With mechanical movement, the printing scale is only limited by mechanical stage range, and the largest area of the nanofilm that can be printed in the prototype machine is 150 * 150 mm². All related printing parameters, including material flow rate, deposition height, and applied voltage, were studied to identify the appropriate settings for desired properties of nanofilms. Conductive PEDOT:PSS-based nanofilms were printed by using the proposed EF-DID as an example. Two types of postprocessing approaches of the EF-DID printed PEDOT:PSS nanofilm including thermal anneals and air dry were applied to treat the nanofilm to get the pure PEDOT:PSS nanofilm. The relation between the morphology of nanoscale structures and process parameters such as deposition time, printing ink constituent, and post-processing approach were studied to improve the fabrication quality of nanofilms. Then functional properties of the EF-DID printed nanofilm, including layer thickness, resistance, and wettability, were evaluated and analyzed to understand how to fabricate transparent PEDOT: PSS nanofilm with the desired property requirements, which are necessary for the further fabrication of solar cells. We believe the presented method would provide a low-cost and highly efficient 3D printing tool that enables the fabrication of next-generation solar cells with different architectures.

Nomenclature	
3D	three dimensional
2D	two dimensional
PEDOT:PSS	poly(3,4-ethylenedioxythiophene)-poly
(styrenesulfonate)	
HTL	hole transport layer
TPP	two-photon polymerization
EF-DID	electrical field-assisted direct ink deposition
DMSO	dimethyl sulfoxide
EHD	electrohydrodynamic
ITO	indium Tin Oxide
IPA	isopropyl alcohol
DIW	direct ink writing
E	electrical field strength
α	liquid radius of the curvature
Н	deposition height
V	applied voltage
μ	dynamic viscosity of the medium
d	diameter of droplet
q	charge of droplet
D	deposition diameter
γ	flow rate
τ	constant
t	deposition time
T_d	deposition thickness
θ	deposition angle

minimum line width

secondary electron microscope

 W_L

SEM

2. Materials and Methods

2.1. Materials preparation

PEDOT: PSS ink in water solution was purchased from Xi'an polymer light corporation. The ink was diluted using DMSO purchased from Sigma Aldrich. Three concentrations (10 wt%, 20 wt%, and 30 wt%) of PEDOT: PSS were dissolved in DMSO for printing purposes. Prepared solutions were sonicated for about 10 mins for better dispersion of PEDOT: PSS nanoparticles. After sonication, solutions were filtered using a 0.45 μ m filter to separate undispersed nanoparticles. All solutions were degassed under a vacuum to remove bubbles before the printing.

2.2. EF-DID printing of nanofilm

Printing inks were directly loaded into a plastic syringe (5 mL, purchased from BD medical), and the plunger of the syringe was mounted on a mechanical linear actuator with a 40 mm movement range (1 μ m resolution, purchased from Parker-Hannifin Corporation) for the material extrusion. A stainless-steel needle with a blunt ending (Bstean 32G ½ inch, 0.09 mm

inner diameter, and 0.25 mm outer diameter) was used to deposit material (Fig.1a). X/Y/Z motions were achieved using mechanical linear stages with a 150 mm movement range (1 μm resolution, purchased from Parker-Hannifin Corporation). A pair of aluminum plates (purchased from BCAMD) were used to mount on the top of stages which moved in both X and Y directions and served as a printing platform. Silicon heating pad (purchase from BCAMD) with an embedded thermistor (NTC 100K thermistor) was attached at the back of the printing platform for the heating treatment. X/Y/Z mechanical linear stages, syringe pump stage, and heating pad were all controlled by Duet 2 control board (purchase from Filastruder), which had modules for stepper motor control, heating control, and thermocouple reading. A RepRap firmware configuration tool was used in the control system and powered by a 12V 30A DC universal regulated switching power supply (purchased from Alitove). HV350REG (purchased from Information Unlimited) was used as the high voltage power supply to generate an electrical field for deposition. Before the fabrication, the indium tin oxide (ITO) glass substrates were sonicated in water, ethanol, isopropyl alcohol (IPA) each for 15 minutes sequentially. After sonication, the substrates are ozoned for 15 minutes to remove any organic impurities.

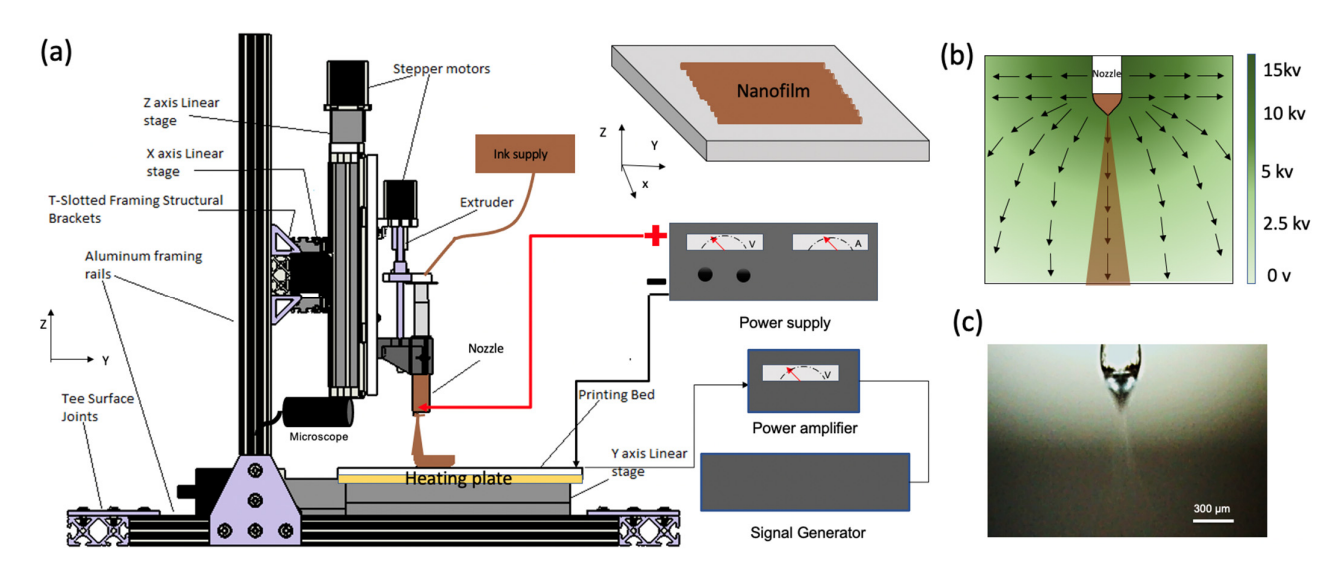


Fig. 1. Schematic illustration of EF-DID process. (a) Schematic diagram of the prototype set-up of EF-DID process; (b) simulation diagram of electrical field around the printing nozzle and the printing bed; and (c) optical microscope image of Taylor cone and charged liquid deposition.

2.3. Design of experiments

For the EF-DID printing process, deposition diameter and functionality of the printed nanofilm are key factors to evaluate. The deposition diameter determines the length of the printing tool path for the large-area fabrication. The functional properties of the printed nanofilm, including layer thickness, electrical conductivity, and wettability are related to the following applications. In EF-DID, printing parameters contain the nozzle-substrate distance, applied voltage, flow rate, solution concentration, deposition time, post-processing method. In order to study the relationships, the following experiments are designed.

Since a stable and uniform deposition is crucial to fabricate nanofilms, the flow rate is adjusted from 0.4 µl/s to 0.8 µl/s to get the optimal surface quality. The deposition diameter is related to the strength of the electrical field, which is determined by the deposition height and the applied voltage. Then two-factor designs method was applied to study the deposition diameter. We decided to use eight deposition heights ranging from 15 mm to 85 mm and three applied voltages (5kv, 10kv, and 15kv). For each combination. 3 samples were prepared and tested. The total number of experimental runs was 72. The properties of printed nanofilms, including the layer thickness, electrical conductivity, wettability, are mainly affected by deposition time, solution concentration, and post-processing method. Therefore, an

experiment was conducted to test the effect of deposition time, solution concentration, and post-processing method. We decided to use three deposition times (8s, 10s, and 15s), three solution concentrations of PEDOT:PSS in DMSO (10 wt%, 20 wt%, and 30 wt%), and two post-process methods (thermal anneal and air-dried) for the experiment design. For each combination. 3 samples were prepared and tested. The total number of experimental runs was 54.

2.4. Post-processing of nanofilm

To remove the solvent, two types of post-processing approaches were tested. In the anneal process, printed films were placed at the heating plate at 130 °C for 15min. In the airdry process, printed films were put inside the fume hood at room temperature for 24 hours.

2.5. Morphology of nanostructures, layer thickness, electrical conductivity, and wettability measurements

Secondary electron microscope analysis was performed on printed nanofilms to evaluate the uniform stability of nanostructures. The layer thickness of printed films was measured with the help of the DEKTAK XT profilometer (provided by ASU Eyring Materials Center). An average of 5 measurements were taken across the entire film. The sheet resistance of the printed films was measured using an Ossila four-point probe, and then the electrical conductivity of the printed nanofilms was calculated based on the measurements. The contact angle of a water droplet on the printed films was conducted to study the wettability using the Minder Hightech SDC-350. The water droplet was firstly dipped on the top surface of the printed nanofilm, and the contact angle of the water droplet was automatically fitted using its software. The resolution of the measurement is within 0.1°.

3. Results and discussion

3.1. Electrical field assisted direct ink deposition

To achieve large-scale fabrication of PEDOT: PSS nanofilms with 2D patterns, we developed a direct ink disposition process with integration of electrical field (Fig. 1a). The schematic diagram of EF-DID consists of X/Y/Z motions, material feeding, heating module, and electrical field generation and control module is shown in Fig. 1a. A highpower supply was utilized, and the power range was from 0 to 35kv. The anode connected deposition nozzle and the cathode connected to the printing bed. An electrical field was formed between the deposition nozzle and the printing bed, and the formed electrical field atomized a liquid solution into a spray of charged nanodroplets. Specifically, the Taylor cone was formed under the nozzle when an electrical field with high voltage was applied between the nozzle and the printing bed (Fig. 1b). The shape of the Taylor cone can be adjusted by modulating the applied voltage. The Taylor cone emitted a liquid jet, and varicose waves on the surface of the jet further generated small and highly charged liquid nanodroplets, which were radially deposited due to coulomb repulsion. As shown in Fig.1c, the liquid jet broke up into the cone-jet mode, and a series of liquid droplets were sprayed at the tip of the cone zone. The deposition of liquid droplets was related to the electric stress and surface tension. The substrate was mounted on the X/Y linear stages to achieve the X/Y movements, which enabled the fabrication of nanofilm with 2D patterns in a largescale area. By controlling the moving speed of the X/Y linear stages, a constant deposition time was determined to print nanofilms.

As shown in Fig.1c, the deposition angle θ maintained the same during the whole printing process, and the deposition diameter D was only linearly related to the deposition height H. However, the deposition density of nanodroplets was reduced with the increase of the deposition height H since the flow rate γ was constant during the printing. The below equation was used to calculate the deposition thickness T_d :

$$T_d = \frac{4\gamma t}{\pi D^2} \tag{4}$$

where the t is deposition time.

After identifying the relationship between the deposition height H and the deposition diameter D, the applied voltage V was varied for each deposition. As shown in Fig. 2c, the increase of applied voltage led to the linear growth of deposition diameter when the deposition distance was set at the same value. However, the flow rate was increased to maintain a stable Taylor cone and achieve stable deposition when the applied voltage was increased. As a result, the higher applied voltage generated a larger deposition angle when the deposition height kept the same value.

3.2. Deposition diameter and flow rate setting

After applying the voltage V, the liquid meniscus generated a semi-spherical shape at the tip of the deposition nozzle, and the electrical field E was induced around the deposition nozzle [27]:

$$E = \frac{2V}{\alpha \ln(4H/\alpha)} \tag{1}$$

where the E is electrical field strength, α is the liquid radius of the curvature, and the H is the deposition height between the printing nozzle and the printing substrate.

The electrical field polarized the liquid during the printing process. When the applied voltage V was above the threshold, the liquid formed the Taylor cone (Fig. 2a). To characterize the deposited liquid, a series of experiments are conducted to identify the relation between printing parameters and properties of nanofilm. The studied printing parameters included applied voltage V of the electrical field and the deposition height H. The velocity of the droplet emitted from the Taylor Zone can be expressed as [28]:

$$v = \frac{Eq}{3\pi\mu d} \tag{2}$$

where μ is the medium's dynamic viscosity in ambient air, d is the diameter of an ink droplet, q is the charge of an ink droplet.

The applied voltage V influenced the emitting speed of droplets from the printing nozzle. Meanwhile, the printing ink was extruded out from the syringe. To achieve stable deposition, the flow rate of nano-ink controlled by the extruder should equal the droplet emitting speed from the Taylor cone. Thus, the flow rate of the ink had to be adjusted accordingly with each applied voltage to maintain a stable Taylor cone. The deposition diameter D was used to evaluate the printing size in the local area, and it was used when planed the tool path for the patternable nanofilm fabrication. The deposition was adjusted by controlling the applied voltage V and deposition height H. Based on the experimental results, the diameter grew linearly as the deposition height H increased. However, the deposition

thickness of the nanofilm was decreased with the increase of the deposition height H. When the applied voltage V was set at 10 kV, the deposition diameters were measured at different deposition heights, ranging from 15 mm to 85 mm. The experimental result of deposition diameters is shown in Fig. 2b. The relation between the deposition diameter D and the deposition height H is shown below:

$$D = \tau H \tag{3}$$

Where τ is constant, and it was 0.1794 when the applied voltage V was set at 10 kV.

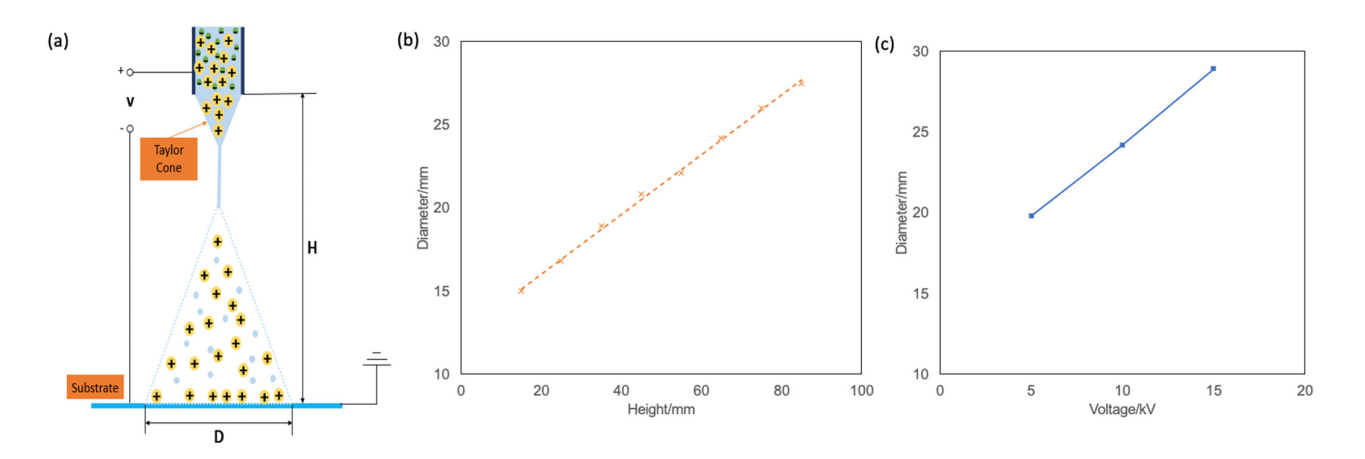


Fig. 2. Schematic illustration of the printing process of electrical field-assisted direct ink deposition. (a) Schematic diagram of deposition during the printing; (b) deposition diameter vs. deposition height; and (c) deposition diameter vs. applied voltage.

3.3. Process planning

Based on the above discussion, the printing process planning of nanofilm with 2D patterns is shown in Fig. 3. For a designed nanofilm with complex 2D patterns, a series of grayscale images were firstly generated by slicing the digital model using a conventional 3D slicing program. The deposition thickness T_d of nanofilm determined the set of layer thickness and further affected the number of deposition layers. The sliced image was then processed, and the minimum line width W_L in the 2D pattern was extracted. The deposition diameter was set the same as the minimum line width W_L . The tool path was fitted to the layer to fill the whole layer, and was generated specifically based on define printing settings, including layer thickness and deposition diameter. Once the deposition diameter was set, the deposition height and the applied voltage were finalized. For example, to print the 30 wt% PEDOT:PSS nanofilm as shown in Fig.3, the minimum line width was set at 25 mm, which was the same as deposition diameter. And then, the flow rate and applied voltages setting were 0.64 µl/s and 10 kV, respectively. After that, moving speeds of X/Y linear stages were determined by deposition height, deposition diameter, and film thickness. Since all the parameters were identified, a series of G codes were generated to print nanofilm with desired morphology of the nano/microstructure. To demonstrate the printing capability of the EF-DID process, a thin PEDOT:PSS nanofilm was deposited on the substrate of flexible paper (Fig.3).

3.4. Nanofilm thickness and electrical conductivity evaluation

Nanofilms were printed onto ITO glass substrates using ink with different concentrations of PEDOT:PSS (10 wt%, 20 wt%, and 30 wt%) in DMSO. The printing parameters, including flow rate, applied voltage, and deposition height, were adjusted according to the concentration of PEDOT: PSS in the printing ink. The nanofilms were printed at flow rates which enabled stable deposition, and different deposition times (8, 10, and 15 sec) were tested to evaluate the thickness. Figure 4 shows thickness measurements results of PEDOT:PSS nanofilms printed using EF-DID with 10 wt%, 20 wt%, and 30 wt% PEDOT:PSS ink, after air-dried and thermal anneals. Postprocessing played an essential role in determining the layer thickness of nanofilms printed by EF-DID at the same conditions. The anneal process further reduced the film thickness, presumably due to loss of water and shrinkage induced by the sintering of the thin film. As shown in Fig. 4a, the nanofilm was printed after 10 sec deposition using PEDOT:PSS inks with different concentrations. The PEDOT:PSS nanofilm thickness after the air dry was much higher than the one after annealing for all nanofilms printed using different concentrations. After the air dry, there is some residual water inside the printed nanofilm, and PEDOT:PSS particles did not grow together as the ones after aneals. Besides,

the thickness of the printed PEDOT:PSS nanofilm grew with the increase of PEDOT:PSS concentration in the printing ink.

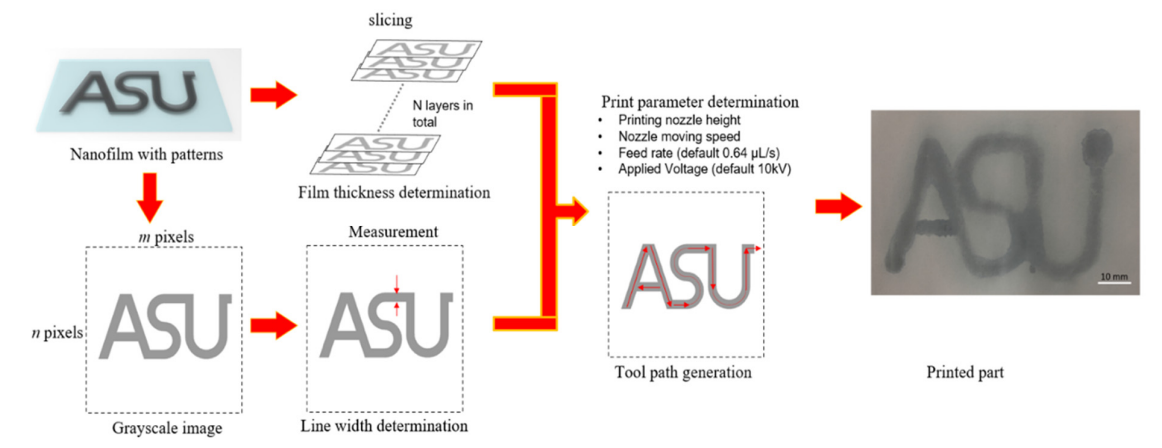


Fig. 3. Schematic illustration of tool path planning for the printing of nanofilms with 2D patterns.

Moreover, the longer deposition time leads to an increase in nanofilm thickness (Fig. 4b). The thickness of annealed nanofilm increased linearly with the increase of the deposition time since the nanofilm thickness was only related to the volume of the deposited PEDOT:PSS for the annealed nanofilm. Moreover, the film thickness of the printed film after the anneal was much more uniform than the one after the air

dry throughout the whole film. The effective resistivity of the EF-DID printed nanofilms was measured, and results are shown in Fig. 4c. After the anneal, the average effective resistivity of the films printed using 10 wt% PEDOT:PSS was 4.15 x $10^4~\Omega\cdot m$. The electrical conductivity of nanofilm printed using 20 wt% PEDOT:PSS solution was better than those printed using 10 and 30 wt% PEDOT:PSS ink (Fig. 4c).

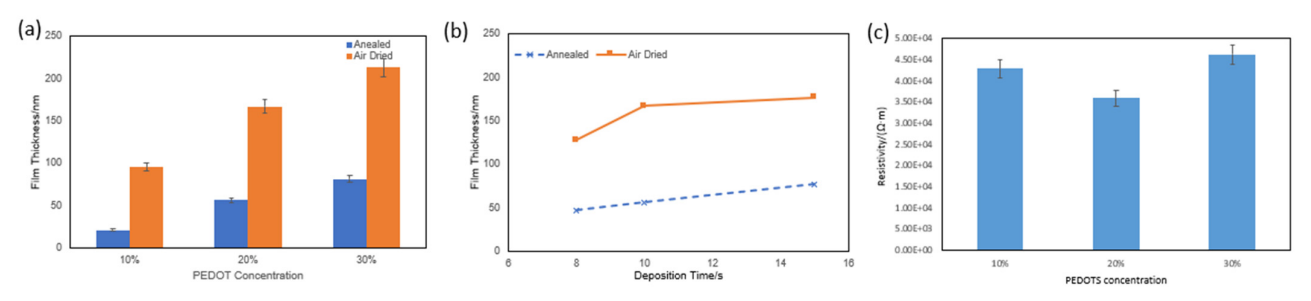


Fig. 4. The layer thickness and resistance of PEDOT:PSS nanofilms printed on ITO glass slides using the EF-DID process. (a) The thickness of PEDOT:PSS nanofilm printed with different concentrations of PEDOT:PSS after post-processing (air-dried and annealed); (b) the thickness of PEDOT:PSS nanofilm printed with different deposition times ranging from 8s to 15s using the 20% PEDOT:PSS ink after post-processing (air-dried and annealed); and (c) the resistance of PEDOT:PSS nanofilm printed using different concentration of PEDOT:PSS after annealed post-processing.

3.5. Morphology evaluation of nanostructures

morphology of the PEDOT:PSS nanostructures was evaluated by surface characterization. The thin films were printed on top of ITO substrates using different concentrations and post-process methods for comparison. Secondary electron microscope (SEM) analysis was performed on EF-DID printed PEDOT:PSS. As shown in Fig. 5(a)-(c), the annealed 20 wt% PEDOT:PSS nanofilms showed the best coverage of smooth and homogenous nanostructures. Compared to the annealed nanofilm, the morphology of nanostructures of air-dried films was inhomogeneous, and there were many pinholes and trap states. The nonannealed film also showed uneven grain boundaries compared to the annealed films. Annealing the EF-DID printed films helped in the evaporation of the solvent, which in turn favored the film formation with the grain growth. Thus, heating the substrates improved the morphology of the EF-DID printed PEDOT:PSS films for homogeneity [11]. For films printed with 10 and 30 wt % PEDOT:PSS ink, we noticed inhomogeneous film formation with pinholes. This indicated a nonuniform distribution of PEDOT:PSS nanodroplets. However, the grain size of PEDOT:PSS particles in the printed nanofilm using 20 wt% PEDOT:PSS ink is much larger than the ones printed using other concentrations. Thus, we considered that the 20 wt% PEDOT:PSS ink would be optimum to build the nanofilm to fabricate the HTL of the solar cell.

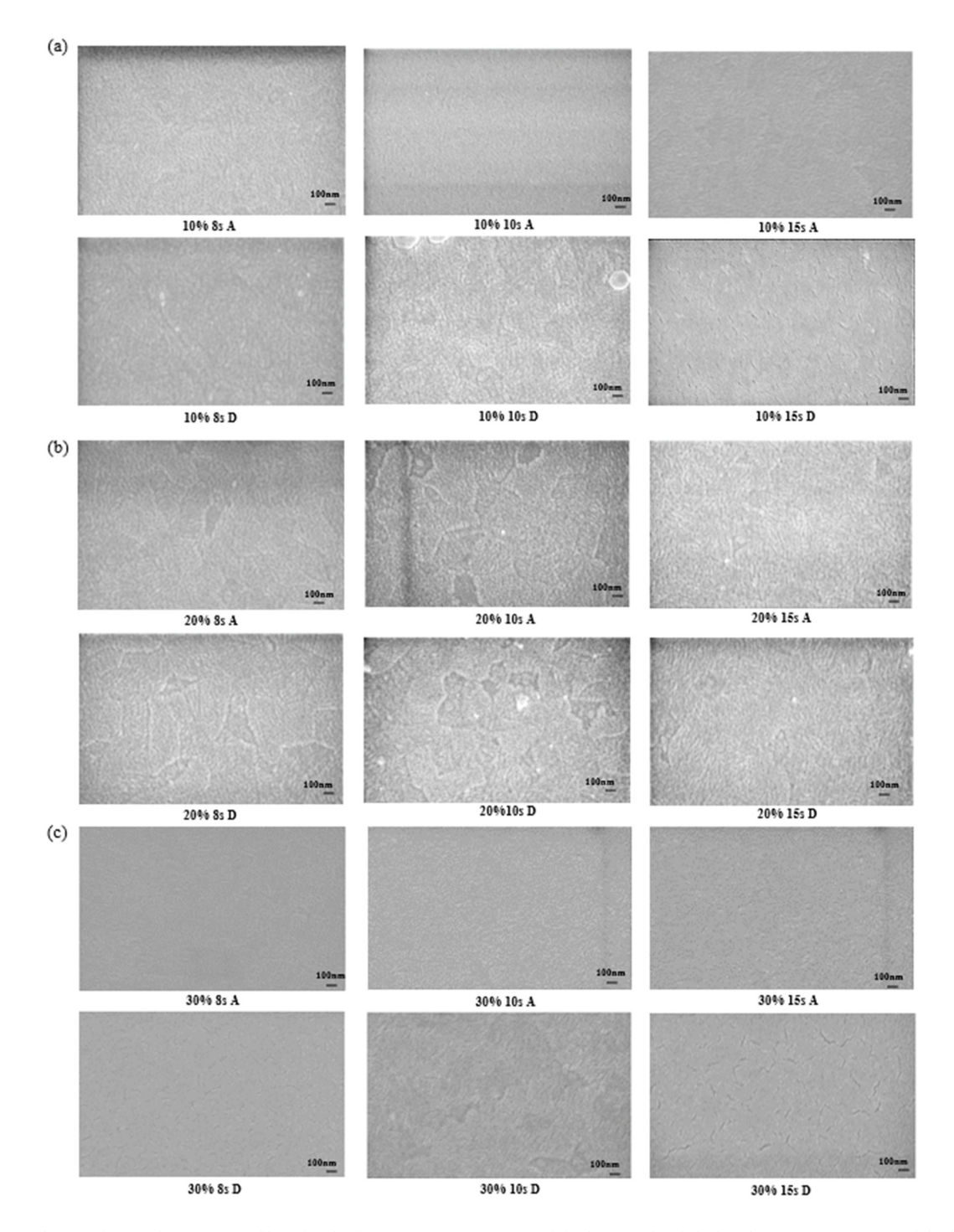


Fig. 5. The SEM image of PEDOT:PSS film printed using (a) 10 wt% PEDOT:PSS ink after anneal and air-dry; (b) 20 wt% PEDOT:PSS ink after anneal and air-dry; and (c) 30 wt% PEDOT:PSS ink after anneal and air-dry.

3.6. Wettability evaluation

Wettability is one of the essential properties of nanofilm for various applications; hence, the contact angle of water droplets on the printed nanofilms was evaluated. A series of nanofilms were printed using different deposition times, PEDOT:PSS concentrations, and post-processing approaches. The contact angles of water droplets on the EF-DID printed nanofilms before and after the post-processing are shown in Fig. 6a. The air-dried nanofilms showed to be more hydrophilic than the annealed films for all deposition times and solution concentrations (Fig. 6b-c). This was because the anneal process evaporated the film's

water more thoroughly. As shown in Fig. 6c, the contact angle of the annealed film printed using 20 wt% PEDOT:PSS ink was the lowest value among all the annealed films since the 20 wt% PEDOT:PSS nanofilm has the best coverage smooth film.

4. Conclusion

A large-scale nanofilm fabrication process, electrical field-assisted direct ink deposition, has been presented, including its

basic concepts, prototype set-up, software implementation, process characteristics, and properties' evaluation. To achieve nanoscale printing, an integrated system consisting of a module creates an electrical field, a material extrusion system, multiaxis motion, and a heating treatment module. A set of experiments have been conducted to identify the optimal printing parameters, including applied voltage, flow rate, and deposition height. The process planning and tool path generation were developed to fabricate nanofilms with 2D spatterns based on the deposition diameter. Functional

properties, such as morphology of nanostructures, layer thickness, electrical conductivity, and wettability were evaluated. The nanofilm printed using 20 wt% PEDOT:PSS ink showed the best performance. Overall, the EF-DID process provides a potential scalable manufacturing tool for the fabrication of functional nanofilms in a highly efficient manner. Furthermore, EF-DID enables the applications of nanofilms for various applications such as flexible electronics, biomedical testing and screening, sustainable energy, robotics, and quantum science [29-31].

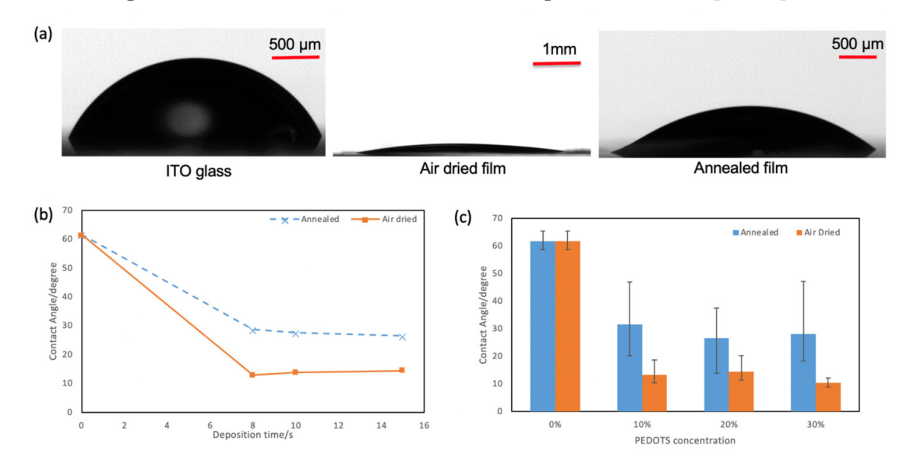


Fig. 6. Wettability of EF-DID printed nanofilms. (a) Microscope images of water droplets on top surface of EF-DID printed nanofilms; (b) the contact angle of EF-DID printed nanofilms using different deposition time and post-processing approach with 20% PEDOT:PSS ink; (c) Contact angle of EF-DID printed nanofilms using different post-processing approaches and inks.

Acknowledgments

Yizhen Zhu and Banashree Gogoi contributed equally to this work. The authors acknowledge Arizona State University Ira A. Fulton Schools of Engineering Strategic Interest Seed Funding and National Science Foundation (NSF grant no. CMMI-2114119). The authors also thank ASU core research facilities for the use of SEM electron microprobe analyzer.

Conflict of Interest

The authors declare no conflict of interest.

References

- References
 Plawsky JL, Fedorov AG, Garimella SV, Ma HB, Maroo SC, Chen L, Nam Y. Nano-and microstructures for thin-film evaporation—A review. Nanoscale and microscale thermophysical engineering. 2014 Jul '3;18(3):251-69.
 Van Zeijl HW. Thin-film technologies for micro/nanosystems; A review. ECS Transactions. 2014 Mar 26;61(3):191.
 Groenendaal L, Jonas F, Freitag D, Pielartzik H, Reynolds JR. Poly (3, 4 ethylenedioxythiophene) and its derivatives: past, present, and future. Advanced materials. 2000 Apr;12(7):481-94.
 Yue R, Xu J, Poly (3, 4-ethylene dioxythiophene) as promising organic thermoelectric materials: A mini-review. Synthetic metals. 2012 Jul 1;162(11-12):912-7.
 Xia Y, Sun K, Chang J, Ouyang J. Effects of organic inorganic hybrid perovskite materials on the electronic properties and morphology of poly (3, 4-ethylenedioxythiophene): poly (styrenesulfonate) and the photovoltaic performance of planar perovskite solar cells. Journal of Materials Chemistry A. 2015;3(31):15897-904.
 Yano H, Kudo K, Marumo K, Okuzaki H. Fully soluble self-doped poly (3, 4-ethylenedioxythiophene) with an electrical conductivity greater than 1000 S cm— I. Science advances. 2019 Apr 1;5(4):eaav9492.
 Ouyang J. "Secondary doping" methods to significantly enhance the conductivity of PEDOT:PSS for its application as transparent electrode of optoelectronic devices. Displays. 2013 Dec 1;34(5):423-36.
 Dong Q, Zhou Y, Pei J, Liu Z, Li Y, Yao S, Zhang J, Tian W. All-spin-coating vacuum-free processed semi-transparent inverted polymer solar cells with PEDOT:PSS anode and PAH-D interfacial layer. Organic Electronics. 2010 Jul 1;11(7):1327-31.
 Je Le JY, Connor ST, Cui Y, Peumans P. Solution-processed metal nanowire mesh transparent electrodes. Nano letters. 2008 Feb 13;8(2):689-92.
 Tahir U, Kamran MA, Jang MH, Jeong MY. Thin-film coating on cylinder for fabrication of cylindrical mold: Roll-to-roll nano-imprint lithography. Microelectronic Engine

- [13] Tuntanatewin W, Tani K, Ishikura K, Zhang H, Okamura Y. One-pot fabrication of polymer micro/nano-discs via phase separation and a roll-to-roll coating process. Colloids and Surfaces A: Physicochemical and Engineering Aspects. 2020 Feb 5;586:124274.
 [14] Yang Y, Song X, Li X, Chen Z, Zhou C, Zhou Q, Chen Y. Recent progress in biomimetic additive manufacturing technology: from materials to functional structures. Advanced Materials. 2018 Sep;30(36):1706559.
 [15] Zhu Y, Joralmon D, Shan W, Chen Y, Rong J, Zhao H, Xiao S, Li X. 3D printing biomimetic materials and structures for biomedical applications. Bio-Design and Manufacturing. 2021 Jan 3:1-24.

- Materials. 2018 Sep;30(36):1706539.
 [15] Zhu Y, Joralmon D, Shan W, Chen Y, Rong J, Zhao H, Xiao S, Li X. 3D printing biomimetic materials and structures for biomedical applications. Bio-Design and Manufacturing. 2021 Jan 3:1-24.
 [16] Li X, Baldacchin T, Song X, Chen Y. Multi-scale additive manufacturing: an investigation on building objects with macro-, micro-and nano-scales features. In 1th International Conference on Micro Manufacturing, Irvine, CA, Mar 2016 Mar 29 (Vol. 29, p. 96).
 [17] Le HP. Progress and trends in inkjet printing technology. Journal of Imaging Science and Technology. 1998 Jan 1;42(1):49-62.
 [18] Liu Y, Huang Y. Theoretical and experimental studies of electrostatic focusing for electrohydrodynamic jet printing. Journal of Micromechanics and Microengineering. 2019 Apr 15:29(6):065002.
 [19] Liashenko I, Rosell-Llompart J, Cabot A. Ultrafast 3D printing with submicrometer features using electrostatic jet deflection. Nature communications. 2020 Feb 6:11(1):1-9.
 [20] Li X, Yang Y, Liu L, Chen Y, Chu M, Sun H, Shan W, Chen Y. 3D Printed Cactus Inspired Spine Structures for Highly Efficient Water Collection. Advanced Materials Interfaces. 2020 Feb;7(3):1901752.
 [21] Li X, Yuan Y, Liu L, Leung YS, Chen Y, Guo Y, Chai Y, Chen Y. 3D printing of hydroxyapatite/tricalcium phosphate scaffold with hierarchical porous structure for bone regeneration. Bio-Design and Manufacturing. 2020 Mar;3(1):15-29.
 [22] Yang Y, Li X, Chu M, Sun H, Jin J, Yu K, Wang Q, Zhou Q, Chen Y. Electrically assisted 3D printing of nacre-inspired structures with self-sensing capability. Science advances. 2019 Apr 1;5(4):eaau9490.
 [23] Li X, Shan W, Yang Y, Joralmon D, Zhu Y, Chen Y, Yuan Y, Xu H, Rong J, Dai R, Nian Q. Limpet Tooth Inspired Painless Microneedles Fabricated by Magnetic Field Assisted 3D Printing. Advanced Functional Materials. 2021 Jan;31(5):2003725.
 [24] Joralmon D, Amonoo E, Zhu Y, Li X. Magnetic Field-Assisted